International Journal of Heat and Mass Transfer 134 (2019) 634–640

Contents lists available at ScienceDirect

International Journal of Heat and Mass Transfer

journal homepage: www.elsevier.com/locate/ijhmt

Effect of nano-film thickness on thermal resistance at water/silicon interface

Onur Yenigun, Murat Barisik *

Department of Mechanical Engineering, Izmir Institute of Technology, Izmir 35430, Turkey

ARTICLE INFO

Article history:
Received 29 October 2018
Received in revised form 27 December 2018
Accepted 17 January 2019
Available online 24 January 2019

Keywords:
Nano-scale heat transfer
Molecular dynamics
Phonon transport
Kapitza resistance

ABSTRACT

Parallel to the developments in micro/nano manufacturing techniques, component sizes in micro/nano electro mechanical systems have been decreasing to nanometer scales. Decrease in lengths in heat transfer direction below the heat carrier phonon length scales reduces thermal conduction in semiconductors. This study shows that such altered phonon spectrums with the decrease of size also reduce the heat transfer at the solid/liquid interfaces and can be correlated with the thermal conductivity of the slab. Using Molecular Dynamics (MD), we measured heat transfer between water and silicon of different thickness between 5 nm and 60 nm. Silicon slabs exhibit a linear temperature profile through the bulk where thermal conductivities measured based on Fourier law decreased by the decreasing slab thickness. We applied a semi-theoretical formulism on variation of conductivity by slab thickness. At the interface of these slabs and water, heat passage is disturbed due to the phonon mismatch of dissimilar materials, which is mostly considered as solid/liquid couple interface properties by the earlier literature. Resistance for phonon passage characterized as Kapitza length (L_K) is measured for different slab thicknesses at different surface wetting conditions varying between hydrophilic to hydrophobic. Increasing surface wetting decreases the L_K while at a certain wetting, decreasing the slab thickness increases the L_K. Once the L_K of different size slabs normalized by its bulk value (assumed to be the L_K of the thickest slab at the corresponding wetting), L_K variation by silicon thickness shows a universal behavior independent of surface wetting. A mathematical model describing the exponential increase of L_K by decreasing thickness was developed and validated by an earlier model. We further developed a correlation between the corresponding changes of L_K and conductivity with respective to their bulk values by analytically combining two models as $(L_K/L_{K-Bulk}) = \exp(3.94(k_{Bulk} - k)/(k \times k_{Bulk}))$, using which L_K can be predicted from available thermal conductivities of a certain material. Results are crucial for thermal management of current and future electronics.

1. Introduction

Developments in nano-fabrication techniques led to the advancement in micro/nano-electronics so transistors as thin as 10 nm can be manufactured by the semiconductor industry [1]. The decrease of the transistor size yields increased packing on a single chip and increased computational power, but also results in extremely high heat generation. If the increase in power density continues similar to the predictions of the Moore's Law, heat generation per area of a microprocessor will reach the heat flux of the sun's surface [2]. Hence, thermal management has become one of the main challenges for the future technologies. Miniaturization bringing the need for removal of high heat fluxes per area also complicates the heat dissipation mechanisms. For such a case, understanding heat conduction in the nanoscale solid parts and heat transfer from nanoscale device components to ambient fluid or coolant through the interfaces is critical to resolve overheating issues.

First, a decrease of solid size alters the heat conduction inside a semi-conductor solid domain which diverges from the conventional bulk scale behavior. This nanoscale size effect is a well-known phenomenon observed both numerically and experimentally by many researchers [3–11] as the decrease of solid thermal conductivity by decreasing length. When the nano-film thickness becomes shorter than the bulk value of the phonon mean free path (MFP), the spectrum of heat-carrying phonons inside the solid domain develops different than the bulk phonon propagation, and the resulted thermal conductivity decreases. This phenomenon

* Corresponding author.
E-mail address: muratbarisik@iyte.edu.tr (M. Barisik).

https://doi.org/10.1016/j.ijheatmasstransfer.2019.01.075
0017-9310/

is a limitation for latent heat removal, but also an interesting tool for heat transfer control by the so-called phonon engineering.

Second, decrease of component sizes in a micro/nano system increases the number of interfaces and their influence. The heat transfer between two dissimilar materials is interrupted due to the mismatch in their phonon spectrum. Such difficulty of phonon passage is characterized by the interface thermal resistance (ITR) which becomes the most dominant mechanism by the increase of surface-to-volume ratio. There are many experimental, theoretical, and computational studies regarding ITR and its dependence on molecular properties [12–26]. However, we are still far from a complete understanding and further studies require for a better design of enhanced heat dissipation.

During the interface heat transfer, the group of phonons approaching the interface show a variety of behavior, some of the phonons pass, some backscatter and some dissipate. The previously discussed literature mostly studied the dependence of ITR onto the material properties at the interface. However, the properties of the phonon package are also expected to strongly influence the ITR. Hence, ITR cannot be a material property only, but also should be affected by the size of the material. Such behavior is studied for solids made of grains smaller than their bulk phonon MFP that grain size dependency of ITR between solid/solid interfaces are examined before [21,27–33]. However, the size dependency of ITR at solid/liquid interfaces has been overlooked in the literature. Earlier, we studied heat transfer between graphene-coated copper and examined the effect of the number of graphene layers on graphene/water ITR [34]. However, there is a need for a broader description of corresponding phonon propagation in a continuous solid and its passage through the interface as a function of solid thickness in a larger scale.

Theoretically, deficiency in overlap between phonon dispersions of different materials can be calculated by The Mismatch Models, where the upper and lower limits of ITR can be predicted by either neglecting phonon scattering or assuming diffuse phonon scattering. But determination of the true ITR value requires calculation of both harmonic and the anharmonic wave behaviors developing in a certain crystal structure with boundaries. For such a case, the coupled motions of the atoms in real space under both intra- and inter-molecular force interactions can be modeled by Molecular Dynamics (MD). MD provides the natural formation and transport of phonons via vibrations in the crystal lattice and has been practiced by many to study heat transport of semiconductors and liquids. Using MD, we presented ITR as a function of surface wetting [34–37], surface temperature [38], surface atomic density [39] and liquid pressure [40] in our earlier work.

Our objective is to examine the heat transfer through the interface between water and silicon nano films of different thicknesses and different surface wettings. Additionally, we will correlate ITR with the thermal conductivity of corresponding silicon film and describe the influence of phonon scattering on both solid and interface thermal transport.

2. Simulation details

We employed non-equilibrium molecular dynamics (NEMD) simulations. Simulation domain consists of water confined between two silicon walls as illustrated in Fig. 1. We varied the silicon wall thickness and performed measurements only on the one side while keeping the other side constant due to the computational limitations. Simulations are conducted with the LAMMPS (Large-scale Atomic/Molecular Massively Parallel Simulator) software. Cross sectional area of the computational domain was 3.8×3.8 nm in the vertical and lateral directions, where periodic boundary conditions were applied. In the longitudinal direction, thickness of the silicon (t) was varied from 5 nm to 60 nm while (0,0,1) crystal plane was facing the fluid. Simulated domains were very large for a classical MD simulation and required extensive computational sources and time.

Water density was kept at 1.006 g/cm^3. SPC/E water model composed of Lennard-Jones and Coulombic potentials is used [41] with SHAKE algorithm to constrain the bond lengths and angles of this rigid model. Stillinger-Weber potential is used for the Si-Si interactions, which considers two-body interactions with an additional many body dependence [42]. The molecular interaction parameters for each molecule pair used in the simulations are given in Tables 1 and 2.

For the silicon-oxygen interactions, parameters can be calculated by the Lorentz-Berthelot (L-B) mixing rule by

$$\sigma_{Si-O} = \frac{\sigma_{Si-Si} + \sigma_{O-O}}{2}, \varepsilon_{Si-O} = \sqrt{\varepsilon_{Si-Si} \times \varepsilon_{O-O}} \quad (1)$$

Using the corresponding parameters given in Table 1, the L-B mixing rule predicts the interaction parameters $\sigma^*_{Si\text{-}O} = 2.6305$ Å and $\varepsilon^*_{Si\text{-}O} = 0.12088$ eV. However, our earlier wetting study based on MD measured contact angles of water nano-droplets showed that

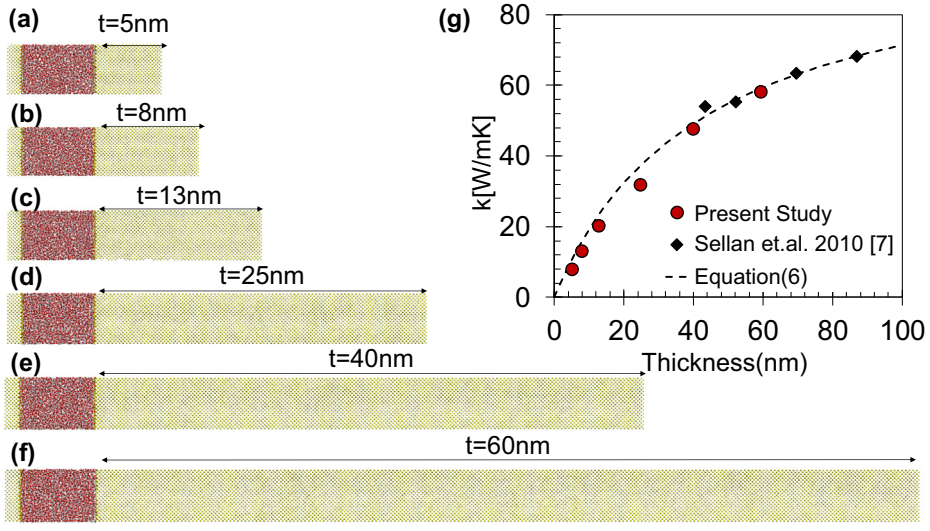

Fig. 1. Simulation domains with different silicon thicknesses (a) 5 nm, (b) 8 nm, (c) 13 nm, (d) 25 nm, (e) 40 nm and (f) 60 nm. (g) Thermal conductivity of silicon varying with nano-film thickness at 500 K.

Table 1
Molecular interaction parameters used in the current study.

Molecule pair	σ (Å)	ε (eV)	q (e)
O-O	3.166	0.006739	−0.8476
H-H	0	0	+0.4238
Si-Si	2.095	2.168201	0

Table 2
Interaction strength values between Silicon and Oxygen.

Molecule pair	$\varepsilon_{Si\text{-}O}/\varepsilon^{*}_{Si\text{-}O}$	$\varepsilon_{Si\text{-}O}$ (eV)
Si-O	1	0.12088
	0.4	0.048352
	0.125	0.015

experimentally measured hydrophobic behavior of silicon surfaces can be recovered when the silicon-oxygen interaction strength is 12.5% of the value predicted using the Lorentz–Berthelot mixing rule [43]. For such a case, we employed this interaction strength value and also further varied interaction strengths (0.125, 0.4 and unity $\varepsilon^{*}_{Si\text{-}O}$) in order to examine the effect of varying surface wetting.

Atoms in the outmost layer of both Silicon walls are fixed to their original locations to maintain a fixed volume system, while the remaining atoms throughout the domain are free to move. A particle-particle particle-mesh (PPPM) solver which can handle long-range Coulombic interactions for periodic systems with slab geometry is used. SPC/E water molecules interact with silicon surface only by van der Waals interactions of silicon and oxygen. By using the Verlet algorithm with a time step of 0.001 ps, Newton's equations of motion were integrated. Simulations were started from the Maxwell-Boltzmann velocity distribution for all molecules at 300 K, while NVT ensemble was applied with Nose Hover thermostat keeping the system at 300 K. To reach an isothermal steady state, initial particle distribution was evolved 3×10^5 time-steps (0.3 ns). Afterwards, the Nose Hover thermostat was applied only on the outmost six layers of the both silicon slabs on the left and right, while the remaining silicon and water molecules in between were free from thermostat at NVE ensemble. The outmost silicon layers on both sides kept at different temperatures to induce heat flux through the thermostat free liquid/solid interfaces. Simulations were performed for an additional 5×10^6 time-steps (5 ns) to ensure that the system attains equilibrium in presence of the heat flux. The computational domain was divided into 100 slab bins with the size of 0.1343 nm for temperature profiles. Smaller bin size, 1200 slab bins with the size of 0.0113 nm, was also employed in order to resolve the fine details of the near wall water density distributions. Time averaging of desired properties are performed through 24×10^6 additional time steps (24 ns).

To compute the heat flux vector for an N particle system, Irving-Kirkwood (I-K) expression is used, while using unity differential operator approximation as follows [44,45],

$$J_k = \frac{1}{Vol}\left\langle \sum_i^N V_k^i \left(E^i + \Phi^i\right) + \sum_{i,j}^N \left(r_k^j + r_k^i\right) W^{i,j} \right\rangle, \tag{2}$$

$$E^i = \frac{1}{2} m^i \left(\left(V_x^i\right)^2 + \left(V_y^i\right)^2 + \left(V_z^i\right)^2 \right), \tag{3}$$

$$W^{i,j} = \frac{1}{2}\left(V_x^i f_x^{i,j} + V_y^i f_y^{i,j} + V_z^i f_z^{i,j} \right), \tag{4}$$

where the first term on the right hand side of Eq. (2) is the kinetic and potential energies carried by particle i, and the second term is the energy transfer to particle i by force interactions with the surrounding particles. In the first term, V_x^i is the peculiar velocity component of particle i in k-direction, while k is the axes of the Cartesian coordinate system; E^i is the kinetic and Φ^i is the potential energy of particle i calculated using Eqs. (3) and (1), respectively. In the second component of Eq. (2), $(r_k^j - r_k^i)$is the kth component of the relative distance vector between particles i and j. The $W^{i,j}$ term is given in Eq. (5), where $f_l^{i,j}$ is the intermolecular force exerted on particle i by particle j in the Cartesian coordinate direction l. An overall heat flux is calculated in the water volume using Eq. (2) by considering the contributions of each atom within a water molecule.

3. Results

The temperature profiles of silicon water sandwich structures are presented in Fig. 2. We applied hot and cold reservoirs to the two ends of each system. While the temperature of the cold reservoirs at the outmost silicon layers on left was kept at 200 K, the temperature of the hot reservoirs at the outmost silicon layers on right was varied between 548 K and 595 K at different system sizes, in order to keep the temperature at the silicon/water interfaces same for every case. Hence, any possible surface temperature effects on ITR was eliminated [38].

Sharp temperature drops were observed inside silicon domain at the interfaces of thermostat applied regions and thermostat free regions. These temperature drops are caused by the phonon alteration in thermostat applied sections due to the dynamic rescaling of the thermostats and named artificial interface thermal resistance [35]. In the thermostat free regions, temperature profiles developed as a result of the free interactions of silicon molecules creating the natural phonon characteristics. The temperature profiles sufficiently away from the interfaces are linear obeying the Fourier's Law. Non-linear temperature profiles are observed in the regions close to the interfaces as a result of phonon backscattering. Extent of this non-continuum region differs by the solid thickness as well.

Thermal conductivity of silicon (k) nano-film is determined by using direct method [7]. We measure the heat flux (q) and the temperature gradient ($\partial T/\partial z$) to estimate thermal conductivities using Fourier's Law of heat conduction ($k = q/(\partial T/\partial z)$). Calculated thermal conductivities at different nano-film thicknesses are shown in Fig. 1g, accompanied with the results from the literature. In Fig. 1g, with decreasing nano-film thickness, thermal conductivity decreases which shows perfect agreement with the literature [7]. With the decrease of the solid thickness in the direction of heat transfer below phonon MFP, heat conduction is no longer developed by diffusive transport, but it includes some ballistic phonon exchange as a function of size. In the ballistic transport, MFP of the phonons are reduced to the length scale of the nanostructure that contribution of shortened path phonons to thermal conductivity reduces [46,47]. A different phonon spectrum develops inside the solid domain as a function of thickness. In addition, thermal conductivity shows a non-linear relation with nano-film thickness as the thickness gets smaller. This non-linear behavior occurs since thermal transport contribution of the phonons whose free paths are reduced to the length scale of the nano-film increases drastically with the decreasing thickness.

We further adopted the theoretical model suggested by Sellan et al. based on Boltzmann transport equation (BTE) and the Matthiessen's rule to describe the size dependency of the thermal conductivity [7]. Their derivation originates from the solution of BTE using a system size dependent relaxation time defined by the intrinsic scatterings and boundary scatterings combined using Matthiessen's rule. Derivations concluded that the size dependence of thermal conductivity can be described as,

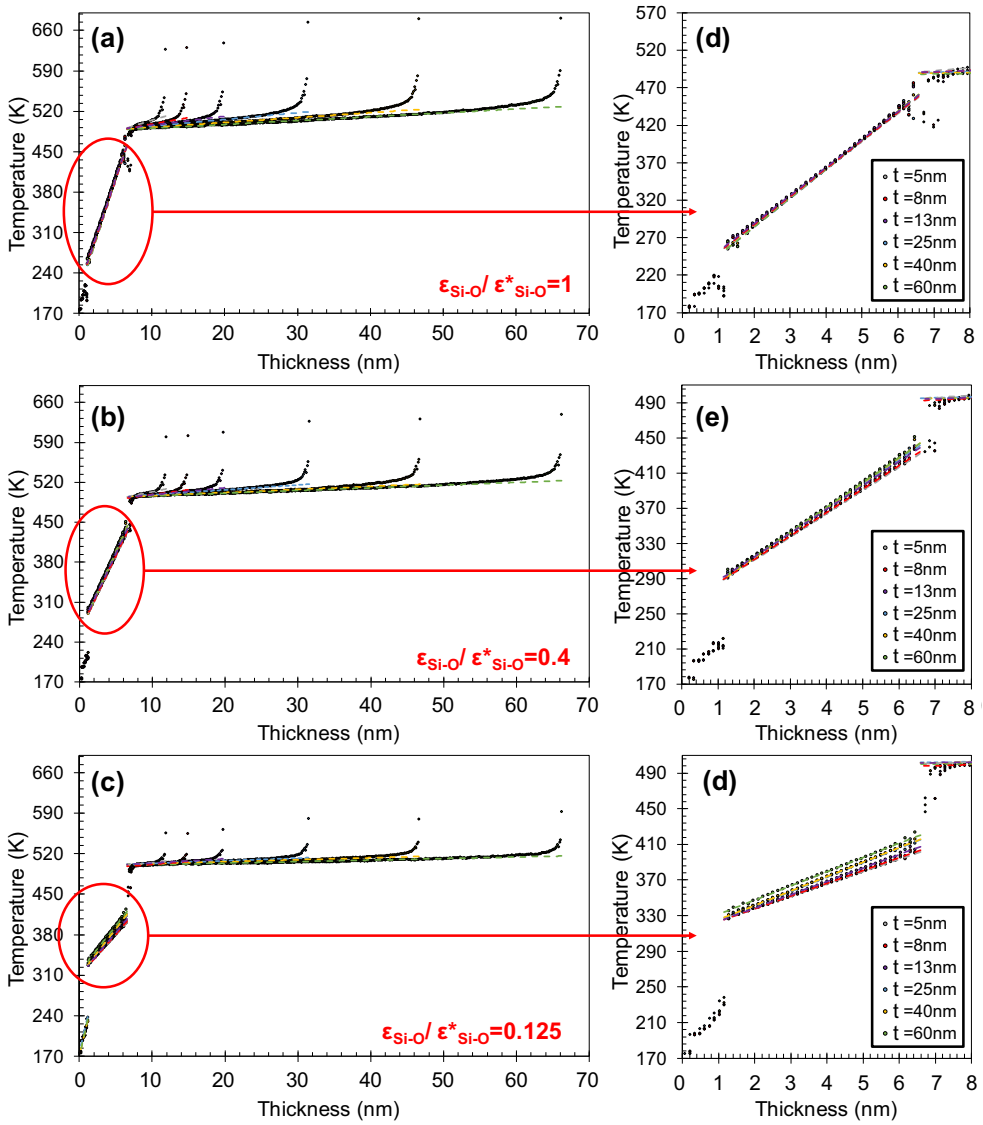

Fig. 2. Temperature distributions of the systems with nano-film thicknesses of 5, 8, 13, 25, 40 and 60 nm with (a) $1.0 \times \varepsilon^*_{Si\text{-}O}$, (b) $0.4 \times \varepsilon^*_{Si\text{-}O}$ and (c) $0.125 \times \varepsilon^*_{Si\text{-}O}$.

$$\frac{1}{k} = \chi\left(\frac{1}{t}\right) \tag{5}$$

where χ was defined as an unknown function of 1/t that converges to $1/k_{Bulk}$ as $1/t \to 0$. This function was calculated using Taylor-series expansion, while the higher order terms were approximated to $1/k_{Bulk}$ after the first order term. We applied Eq. (5) onto the results presented in Fig. 1g and obtained the following semi-theoretical and empirical model for size dependent conductivity as,

$$\frac{1}{k} = 0.43\frac{1}{t} + \frac{1}{k_{Bulk}} \tag{6}$$

where k is the thermal conductivity, k_{Bulk} is the bulk thermal conductivity (taken as 102 W/mK at 500 K [7]), and t is the thickness of the silicon slab. The dashed line given in Fig. 1g representing the Eq. (6) shows good agreement with the calculated data.

In the water domain, temperature profiles are linear except the near wall regions, where temperature profile fluctuates due to the density layering created by the surface forces. This density layering is a function of surface wettability and has a strong impact on ITR [38]. The closer views of the near surface water density layering at different surface wetting conditions are given in Fig. 3. First, near surface water shows two density layers and penetration between the first and second silicon layers. The nearest density peak and penetration increases with the increase of water/silicon interaction strength. But for a given interaction strength, water density profiles near the different thickness silicon slabs are found identical. In all cases, water density reaches its bulk value of 1.006 g/cm^3.

Temperature jumps at the silicon/water interface are measured for various size silicon systems and wetting conditions. The mismatch in the phonon spectrum of silicon and water pair creates this temperature jump which can also be characterized by Kapitza Length (L_K) as in Eq. (6).

$$\Delta T = L_K \left.\frac{\partial T}{\partial n}\right|_{liquid}, \tag{7}$$

where $\partial T/\partial n$ is the temperature gradient of the liquid and ΔT is the temperature jump at the liquid/solid interface. Kapitza length values of different nanofilm thicknesses for different surface wettings are documented in Table 3.

In Fig. 4, variation of L_K with respect to different surface wetting and nanofilm thickness are given to show the trend. In Fig. 4a, L_K decreases with increasing interaction strength due to the stronger

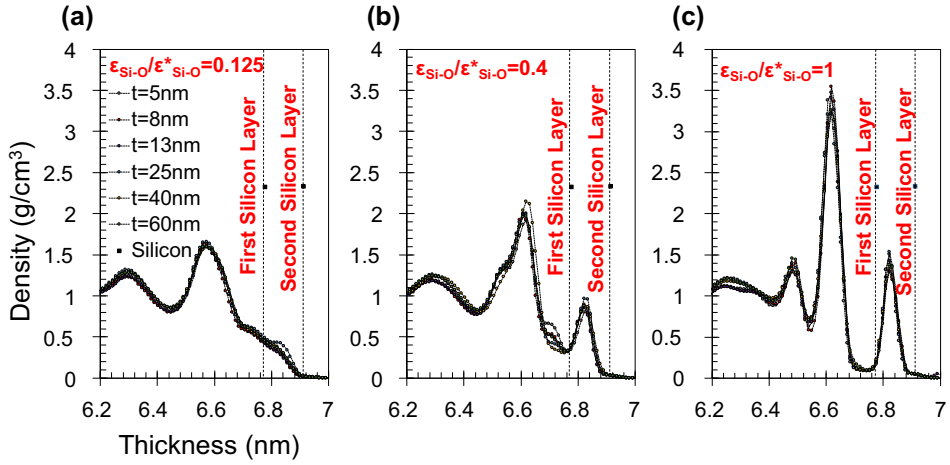

Fig. 3. Near wall density profiles of different nano-film thicknesses at different interaction parameters of (a) $0.125 \times \varepsilon^*_{Si\text{-}O}$, (b) $0.4 \times \varepsilon^*_{Si\text{-}O}$ and (c) $1 \times \varepsilon^*_{Si\text{-}O}$.

Table 3
Kapitza length values measured at different nanofilm thicknesses and at different surface wettings.

	Kapitza length (L_K) [nm]		
Thickness [nm]	$\varepsilon_{Si\text{-}O}/\varepsilon^*_{Si\text{-}O} = 0.125$	$\varepsilon_{Si\text{-}O}/\varepsilon^*_{Si\text{-}O} = 0.4$	$\varepsilon_{Si\text{-}O}/\varepsilon^*_{Si\text{-}O} = 1$
5	7.158	2.394	0.926
8	6.612	2.199	0.853
13	6.290	2.053	0.828
25	5.375	1.939	0.775
40	5.304	1.801	0.725
60	4.996	1.799	0.700

coupling between water and silicon. Increase of water density peaks near the silicon walls by increasing the interaction strength observed from Fig. 3 describes this increased molecular coupling at the interface. We also measured the contact angles which can describe the variation from hydrophobic to hydrophilic behavior by the increase of interface interaction strength, which also describes the increase of interface coupling. At a certain interaction strength, L_K shows variation by the silicon thickness. Decrease of nano-film thickness increases the L_K. Since surface temperatures and near surface water density layers are identical for all these different size silicon cases, variation in ITR is solely due to the change in phonon spectrum by the change in thickness. Variation of L_K by silicon thickness is prominent at low surface wetting but becomes indistinguishable in Fig. 4a with the increase of surface wetting. Instead, comparable L_K variation by silicon thickness is presented by normalizing L_K values with the bulk L_K of corresponding interaction strength. Since the variation of L_K is negligible after silicon thickness becomes 40 nm and higher, we assumed that $L_{K\text{-}60nm}$ of each interaction strength is the bulk value of corresponding case. Variation of normalized L_K at different surface wettings given in Fig. 4b shows very similar behavior by the change of silicon thickness. Compared to their bulk silicon value, L_K shows strong dependence on the nano-film thickness. L_K increases exponentially by the decrease in nano-film size. A similar size dependency of thermal resistance has been reported for the case of solid/solid interfaces previously [27–33]. Variation of normalized L_K by the change in film thickness is found almost independent from surface energy.

In order to characterize the observed variation, we applied a mathematical fit to the normalized Kapitza length values. An exponential variation with the inverse power of silicon thickness described the behavior of L_K well as;

$$\frac{L_K}{L_{K-Bulk}} = \exp\left(\frac{1.7}{t}\right) \tag{8}$$

We tested current model with the earlier L_K model developed for temperature dependence of L_K using a 3.5 nm thick silicon slab [38]. Prediction of current model for the L_K of 3.5 nm thick silicon slab match well with the prediction of the earlier model for 490 K silicon surface with an error less than 18%. This also showed the possible complementary behavior of two models developed by our group. These two models together can predict interface heat transfer as a function of surface temperature and slab thickness.

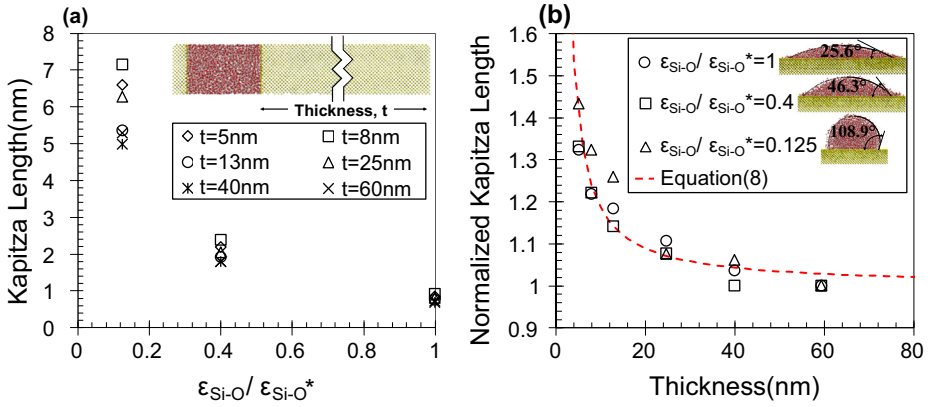

Fig. 4. (a) Variation of Kapitza Length by interaction strength. (b) Variation of Kapitza Length normalized with bulk L_K (60 nm nano-film) by nano-film thickness.

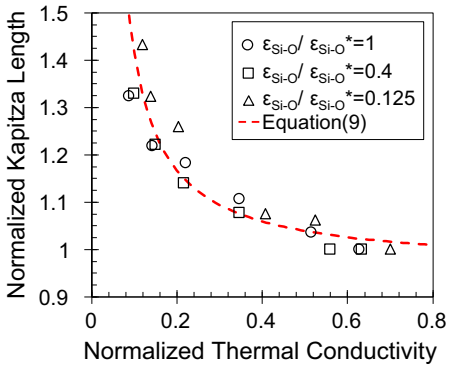

Fig. 5. Variation of Kapitza Length normalized with bulk L_K (60 nm nano-film) by thermal conductivity normalized with bulk k [7].

The behavior observed in Fig. 4b is independent of surface wetting suggesting that the variation of L_K by slab thickness is purely due to the variation in phonon dynamics. In this extent, Eq. (7) provides an L_K model specific for silicon/water couple as the measured slab thickness dependent variation in phonon dynamics was belong to silicon material. Different solids will develop different variation in phonon dispersion by slab thickness, which can be directly deduced from corresponding thermal conductivity behavior. Hence, rather than an L_K description based on slab thickness (material specific), correlating L_K variation with the corresponding variation in thermal conductivity by slab thickness can provide a more general description. With this objective, we analytically combined Eqs. (6) and (8), describing variation of k and L_K by slab thickness, as;

$$\frac{L_K}{L_{K-Bulk}} = \exp\left(\frac{3.94}{k_{Bulk}}\left(\frac{k_{Bulk}}{k} - 1\right)\right) \tag{9}$$

Eq. (9) directly correlates the L_K with the corresponding phonon dynamics in terms of thermal conductivity. Next, we plotted calculated the normalized L_K values at their corresponding normalized thermal conductivities in Fig. 5 and tested Eq. (9). Predictions of our model agreed very well with the data.

The change in phonon characteristics influences L_K and k at different levels; the increase rate of L_K from its bulk value is much higher than decrease rate of conductivity from its bulk value. On the other hand, L_K converges to its bulk value very slowly that it reaches values very close to $L_{K\text{-}Bulk}$ a lot earlier than k; $L_K/L_{K\text{-}Bulk} \approx 1$ while $k/k_{Bulk} \approx 0.5$. Overall, decrease in length scales develops different effects in phonon dynamics of different materials, but variation in phonon distribution shows itself through the variation of conductivity. Also, the size dependent behavior of L_K is independent from surface wetting that effect of altered phonon dynamics on L_K can directly be predicted from the variation in thermal conductivity using Eq. (9). Furthermore, the thermal conductivity as a function of size is available for several materials that L_K can be easily calculated from them using our model.

4. Conclusions

Our results showed that the solid thermal conductivity decreases with the decreasing nano-film thickness. Altered phonon spectrum developing inside silicon as a function of nano-film thicknesses creates a size dependency on thermal conductivity. For such a case, we presented that the variation in phonon distribution also effects heat transport at the interface. Since the approaching phonon spectrum was changed, their passage through the interface also altered. We observed that increased ballistic phonon transport decreases the interface heat transfer as it decreases the thermal conductivity. We characterized the thermal resistance at the interface by the Kapitza length, which experienced an exponential increase by the decrease of slab thickness. L_K decreased when we change surface wetting from hydrophobic to hydrophilic, but variation of normalized L_K by slab thickness showed a universal behavior. Based on the MD measurements, we developed a phenomenological model which successfully predicted L_K values from another study. Finally, we correlated the increase of L_K with the decrease of thermal conductivity which can provide L_K values for the cases where thermal conductivity of nano-slab is known. The results of this study are essential for designing heat removal mechanisms at nano-scale systems.

Conflict of interest

The authors declare no competing interests.

Acknowledgements

This work was supported by the Turkish Academy of Sciences (TUBA) in the framework of the Young Scientist Award Programme (GEBIP).

References

[1] C. Auth, A. Aliyarukunju, M. Asoro, D. Bergstrom, V. Bhagwat, J. Birdsall, N. Bisnik, M. Buehler, V. Chikarmane, G. Ding, Q. Fu, H. Gomez, W. Han, D. Hanken, A 10nm high performance and low-power CMOS technology featuring 3rd generation FinFET transistors, Self-Aligned Quad Patterning, contact over active gate and cobalt local interconnects, International Electron Devices Meeting (IEDM), IEEE, 2017. https://doi.org/10.1109/IEDM.2017.8268472.
[2] X. Zhang, Z.-Y. Guo, Micro/nanoscale heat transfer: interfacial effects dominate the heat transfer, Third International Conference on Micro/Nanoscale Heat and Mass Transfer, ASME, 2012. https://doi.org/10.1115/MNHMT2012-75355.
[3] M. Asheghi, M.N. Touzelbaev, K.E. Goodson, Y.K. Leung, S.S. Wong, J. Heat Transfer-Trans. Asme 120 (1998) 30–36, https://doi.org/10.1115/1.2830059.
[4] Y.S. Ju, K.E. Goodson, Appl. Phys. Lett. 74 (20) (1999) 3005–3007, https://doi.org/10.1063/1.123994.
[5] P.K. Schelling, S.R. Phillpot, P. Keblinski, Phys. Rev. B 65 (2002) 14, https://doi.org/10.1103/PhysRevB.65.144306.
[6] W. Liu, M. Asheghi, Appl. Phys. Lett. 84 (19) (2004) 3819–3821, https://doi.org/10.1063/1.1741039.
[7] D.P. Sellan, E.S. Landry, J.E. Turney, A.J.H. McGaughey, C.H. Amon, Phys. Rev. B 81 (2010) 21, https://doi.org/10.1103/PhysRevB.81.214305.
[8] Y. Ma, Appl. Phys. Lett. 101 (2012) 21, https://doi.org/10.1063/1.4767337.
[9] Y. Dong, B.-Y. Cao, Z.-Y. Guo, Phys. E: Low-Dimens. Syst. Nanostruct. 56 (2014) 256–262, https://doi.org/10.1016/j.physe.2013.10.006.
[10] M. Frank, D. Drikakis, N. Asproulis, Thermal conductivity of nanofluid in nanochannels, Microfluid. Nanofluid. 19 (5) (2015) 1011–1017, https://doi.org/10.1063/1.4949270.
[11] K. Hyżorek, K.V. Tretiakov, Thermal conductivity of liquid argon in nanochannels from molecular dynamics simulations, J. Chem. Phys. 144 (19) (2016) 194507, https://doi.org/10.1007/s10404-015-1591-3.
[12] G.L. Pollack, Rev. Mod. Phys. 41 (1) (1969) 48–81, https://doi.org/10.1103/RevModPhys. 41.48.
[13] J.D.N. Cheeke, Le Journal de Physique Colloques 31 (C3) (1970), https://doi.org/10.1051/jphyscol: 1970312, C3–129-C3-136.
[14] L. Xue, P. Keblinski, S.R. Phillpot, S.U.S. Choi, J.A. Eastman, Int. J. Heat Mass Transfer 47 (19–20) (2004) 4277–4284, https://doi.org/10.1016/j.ijheatmasstransfer.2004.05.016.
[15] Z. Ge, D.G. Cahill, P.V. Braun, Phys. Rev. Lett. 96 (18) (2006) 186101, https://doi.org/10.1103/PhysRevLett. 96.186101.
[16] B. Kim, A. Beskok, T. Cagin, J. Chem. Phys. (2008) 129, https://doi.org/10.1063/1.3001926.
[17] B.H. Kim, A. Beskok, T. Cagin, Microfluid. Nanofluid. 5 (4) (2008) 551–559, https://doi.org/10.1007/s10404-008-0267-7.
[18] S. Murad, I.K. Puri, Chem. Phys. Lett. 467 (1–3) (2008) 110–113, https://doi.org/10.1016/j.cplett.2008.10.068.
[19] L.A. Jauregui, Y. Yue, A.N. Sidorov, J. Hu, Q. Yu, G. Lopex, R. Jalilian, D.K. Benjamin, D.A. Delk, W. We, Z. Liu, X. Wang, Z. Jiang, Y.P. Chen, ECS Trans. 5 (28) (2010) 73–83, https://doi.org/10.1149/1.3367938.
[20] B. Kim, Chem. Phys. Lett. 554 (2012) 77–81, https://doi.org/10.1016/j.cplett.2012.10.022.
[21] Z. Liang, K. Sasikumar, P. Keblinski, Phys. Rev. Lett. 113 (6) (2014) 065901, https://doi.org/10.1103/PhysRevLett. 113.065901.
[22] T.Q. Vo, B. Kim, Sci. Rep. 6 (2016) 33881, https://doi.org/10.1038/srep33881.

[23] T.Q. Vo, B. Kim, J. Chem. Phys. 148 (3) (2018) 034703, https://doi.org/10.1063/1.5004545.
[24] J. Vera, Y. Bayazitoglu, Temperature and heat flux dependence of thermal resistance of water/metal nanoparticle interfaces at sub-boiling temperatures, Int. J. Heat Mass Transfer 86 (2015) 433–442, https://doi.org/10.1016/j.ijheatmasstransfer.2015.02.033.
[25] G. Song, C. Min, Temperature dependence of thermal resistance at a solid/liquid interface, Mol. Phys. 111 (7) (2013) 903–908, https://doi.org/10.1080/00268976.2012.756990.
[26] D. Alexeev, J. Chen, J.H. Walther, K.P. Giapis, P. Angelikopoulos, P. Koumoutsakos, Kapitza resistance between few-layer graphene and water: liquid layering effects, Nano Lett. 15 (9) (2015) 5744–5749, https://doi.org/10.1021/acs.nanolett.5b03024.
[27] S.W. Chang, A.K. Nair, M.J. Buehler, J. Phys. Condens. Matter 24 (24) (2012) 245301, https://doi.org/10.1088/0953-8984/24/24/245301.
[28] S. Merabia, K. Termentzidis, Phys. Rev. B 86 (2012) 9, https://doi.org/10.1103/PhysRevB.86.094303.
[29] R.E. Jones, J.C. Duda, X.W. Zhou, C.J. Kimmer, P.E. Hopkins, Appl. Phys. Lett. 102 (2013) 18, https://doi.org/10.1063/1.4804677.
[30] Z. Liang, P. Keblinski, Phys. Rev. B 90 (2014) 7, https://doi.org/10.1103/PhysRevB.90.075411.
[31] T. Meier, F. Menges, P. Nirmalraj, H. Holscher, H. Riel, B. Gotsmann, Phys. Rev. Lett. 113 (6) (2014) 060801, https://doi.org/10.1103/PhysRevLett. 113.060801.
[32] J. Yang, M. Shen, Y. Yang, W.J. Evans, Z. Wei, W. Chen, A.A. Zinn, Y. Chen, R. Prasher, T.T. Xu, P. Keblinski, D. Li, Phys. Rev. Lett. 112 (2014) 20, https://doi.org/10.1103/PhysRevLett. 112.205901.
[33] Y. Tao, C. Liu, W. Chen, S. Cai, C. Chen, Z. Wei, K. Bi, J. Yang, Y. Chen, Phys. Lett. A 381 (22) (2017) 1899–1904, https://doi.org/10.1016/j.physleta.2017.03.020.
[34] A.T. Pham, M. Barisik, B. Kim, Int. J. Heat Mass Transf. 97 (2016) 422–431, https://doi.org/10.1016/j.ijheatmasstransfer.2016.02.040.
[35] M. Barisik, A. Beskok, J. Comput. Phys. 231 (23) (2012) 7881–7892, https://doi.org/10.1016/j.jcp.2012.07.026.
[36] Z. Shi, M. Barisik, A. Beskok, Int. J. Therm. Sci. 59 (2012) 29–37, https://doi.org/10.1016/j.ijthermalsci.2012.04.009.
[37] A.T. Pham, M. Barisik, B. Kim, Int. J. Precis. Eng. Manuf. 15 (2) (2014) 323–329, https://doi.org/10.1007/s12541-014-0341-x.
[38] M. Barisik, A. Beskok, Int. J. Therm. Sci. 77 (2014) 47–54, https://doi.org/10.1016/j.ijthermalsci.2013.10.012.
[39] T.Q. Vo, M. Barisik, B. Kim, J. Chem. Phys. 144 (19) (2016) 194707, https://doi.org/10.1063/1.4949763.
[40] A. Pham, M. Barisik, B. Kim, J. Chem. Phys. 139 (24) (2013) 244702, https://doi.org/10.1063/1.4851395.
[41] H.J.C. Berendsen, J.R. Grigera, T.P. Straatsma, J. Phys. Chem. 91 (24) (1987) 6269–6271, https://doi.org/10.1021/j100308a038.
[42] F.H. Stillinger, T.A. Weber, Phys. Rev. B 31 (8) (1985) 5262–5271, https://doi.org/10.1103/PhysRevB.31.5262.
[43] M. Barisik, A. Beskok, Mol. Simul. 39 (9) (2013) 700–709, https://doi.org/10.1080/08927022.2012.758854.
[44] J.H. Irving, J.G. Kirkwood, The statistical mechanical theory of transport processes. IV. The equations of hydrodynamics, J. Chem. Phys. 18 (6) (1950) 817–829, https://doi.org/10.1063/1.1747782.
[45] B.D. Todd, P.J. Daivis, D.J. Evans, Heat flux vector in highly inhomogeneous nonequilibrium fluids, Phys. Rev. E 51 (5) (1995) 4362, https://doi.org/10.1103/PhysRevE.51.4362.
[46] Y. Dong, B.-Y. Cao, Z.-Y. Guo, Phys. E: Low-Dimens. Syst. Nanostruct. 66 (2015) 1–6, https://doi.org/10.1016/j.physe.2014.09.011.
[47] J. Lee, J. Lim, P. Yang, Nano Lett. 15 (5) (2015) 3273–3279, https://doi.org/10.1021/acs.nanolett.5b00495.